

## Prediction of pore facies using GMDH-type neural networks: a case study from the South Pars gas field, Persian Gulf basin

Ebrahim Sfidari<sup>1,5</sup>, Ali Kadkhodaie<sup>2\*</sup>, Behzad Ahmadi<sup>3</sup>, Bahman Ahmadi<sup>4</sup>, Mohammad Ali Faraji<sup>5</sup>

<sup>1</sup> Petroleum Geology research group, Research Institute of Applied Sciences, ACECR

<sup>2</sup> Department of Earth Science, Faculty of Natural Science, University of Tabriz, Tabriz, Iran

<sup>3</sup> Department of mechanical engineering, Sharif University of technology, Tehran, Iran

<sup>4</sup> Department of mechanical engineering, University of Guilan, Rasht

<sup>5</sup> Department of Geology, University College of Sciences, University of Tehran, Tehran, Iran

\*Corresponding author, e-mail: kadkhodaie\_ali@tabrizu.ac.ir

(received: 01/03/2017 ; accepted: 04/12/2017)

### Abstract

Pore facies analysis plays an important role in the classification of reservoir rocks and reservoir simulation studies. The current study proposes a two-step approach for pore facies characterization in the carbonate reservoirs with an example from the Kangan and Dalan formations in the South Pars gas field. In the first step, pore facies were determined based on Mercury Injection Capillary Pressure (MICP) data in corporation with the Hierarchical Clustering Analysis (HCA) method. Each pore facies represents a specific type of pore geometry indicating the interaction between the primary rock fabric and its diagenetic overprints. In the next step, polynomial meta-models were established based on the evolved Group Method of Data Handling (GMDH) neural networks for the purpose of pore facies identification from well log responses. In this way, the input data table used for training GMDH-type neural network consists of CALI, GR, CGR, SGR, DT, NPFI, RHOB, PEF, PHIE and VDL logs. The MICP-HCA derived pore facies were considered as the desired outputs. Moreover, multi-objective genetic algorithms (GAs) are used to evolutionary design of GMDH-type neural networks. Training error and prediction error of neural network have been considered as conflicting objectives for Pareto multi-objective optimization. The results of this study indicate the successful implementation of GMDH neural networks for classification of pore facies in the heterogeneous gas bearing carbonate rocks of South Pars gas field.

**Keywords:** Pore Facies, MICP Curves, Clustering, Classification, GMDH, Multi-Objective Optimization, South Pars Gas Field

### Introduction

Carbonate reservoirs are more complicated compared to clastic rock counterparts. At reservoir scale, carbonate porosity rarely follows depositional facies boundaries due to the extensive influence of diagenesis. At pore scale carbonate reservoirs may be very heterogeneous because they have been influenced by a variety of depositional and diagenetic processes (Ahr, 2008). Due to these heterogeneities, hydrocarbon storage, production and recovery in carbonate reservoirs is very complex. Pore-size is the common link between permeability and hydrocarbon saturation. Permeability models have historically described pore space in terms of the radius of a series of capillary tubes (Lucia, 2007). Kozeny (1927) substituted surface area of the pore space for pore radius and afterward, Carman (1956) developed the well-known Kozeny-Carman equation relating permeability to porosity. Pore-size distribution is important along with porosity in estimating permeability. In general, it can be concluded that there is no relationship between porosity and permeability in carbonate rocks unless the pore-size distribution is included (Lucia, 2007). Capillary

pressure as the difference in pressure across the interface between two phases has a significant role in oil flow. Capillary pressure curves contain valuable information about pore systems and are very useful in predicting production capacities (Chehrazi *et al.*, 2011). Extracting such information as rock parameters and then classifying or clustering these parameters into various groups can give important details on carbonates permeability and production capability. Parameters such as pore throat radius, pore throat sorting and height above free water level can be derived from these curves. Some studies proposed Rock typing based on pore typing using MICP test (Kopaska-Merkel *et al.* 1989; Marzouk *et al.*, 1995; Skalinski *et al.*, 2005) and nuclear magnetic resonance (NMR) T2 cutoffs incorporation with MICP test (Arfi *et al.* 2006; Vincent *et al.*, 2011). Proposed pore facies based on pore typing using MICP test was achieved in cored wells. (Chehrazi *et al.*, 2011). Pore facies prediction in uncored wells based on wireline logs is a challenging subject. In this way, pore facies is similar to other facies definitions. Several approaches have been proposed in literature for electrofacies (e.g. Rogers *et al.*, 1992; Serra *et al.*,

1985; Sfidari *et al.*, 2012; Sfidari *et al.*, 2014; Wolff and Pelissier -Combescure, 1982) lithofacies prediction (Ma *et al.*, 2014; Perez *et al.*, 2003; Saggaf & Nebrija, 2000; Tang & Ji, 2006) and pore facies in cored wells (Chehrizi *et al.*, 2001).

The main scope of this paper is porefacies definition at cored sections based on MICP curves and prediction of a set of predefined facies for uncored wells. In the current study, firstly, MICP parameters were derived and clustered by using HCA method and the resulting pore facies were then estimated from conventional well logs by using the GMDH-type neural networks in the South Pars Gas field. In this research, multi-objective genetic algorithms are used to optimal design of the generalized structure of GMDH-type (GS-GMDH) neural network (Jamali *et al.*, 2009; Nariman-Zadeh *et al.*, 2005) in which connectivity configuration in such networks is not limited to adjacent layers for modelling, classification and estimation in some applications.

The objective functions in optimal design of GS-GMDH are, namely, training error and prediction error which should be minimized simultaneously. Therefore, optimal Pareto set of such GMDH are obtained which represent the compromise between the objective functions. Consequently, the best compromise solution is selected from the Pareto optimal set. By this way, some input–output data consisting of sample parameters as inputs and pore facies as output are used for training such GMDH-type neural networks. For the purpose of demonstrating the prediction capability of designed GMDH-type neural network, input–output data set have been divided into two separate sets, namely, training and testing sets. The training set which consists of selected input–output dataset is used for training the neural network using the evolutionary algorithms.

The testing set which consists of remaining unforeseen input–output data samples during the training process is merely used for testing to demonstrate the prediction capability of such evolved GMDH-type neural network models during the training process (Jamali *et al.*, 2013). In former studies, capillary pressure ( $P_c$ ) derived parameters have been used for pore facies identification and interpretation of pore size characteristics so that they suffer severely from core data scarcity. However, we need to propagate reservoir pore facies for all logged and uncored wells. Of course, intelligent systems have widely been used for

estimation of reservoir parameters (e.g. Kadkhodaie-Ilkhchi *et al.*, 2009; Mohaghegh, 2005; Rezaee *et al.*, 2007; Rolon *et al.*, 2009), pore facies characterization is still a challenging issue. The current study bridges core derived pore size characteristics and well logging data by using GMDH-type NNs and it tries to estimate pore facies for all logged but not cored wells which will then be used for the construction of reservoir static model.

### Geological setting

The Persian Gulf basin, as one of the largest petroleum provinces in the world, is located between the Zagros belt and Arabian shield. This region has evolved through different tectonic processes, which resulted in forming numerous petroleum systems with the significant source, reservoir and cap rocks.

The South Pars Gas Field with 441.5 tcf proved reserve with its Qatari extension, North Field with 900.5 tcf gas in place is the largest non-associated gas field in the world. Gas accumulation in this field is restricted to the Upper Permian to Early Triassic carbonates of Kangan and Dalan formations which are time equivalent of Khuff Formation in the Arabian plate. The formations are related to the opening stage of the Neo-Tethys Ocean in the region followed by regional epirogenic movements of the Qatar Arch. (Ghazban, 2007).

The structure of the SPGF is part of the gigantic NE–SW trending Qatar Arch. Its regional geology and reservoir characteristics is well documented in numerous publications (Kashfi, 1992; Alsharhan & Naim, 1997; Insalaco *et al.*, 2006; Ehrenberg *et al.*, 2007; Rahimpour-Bonab *et al.*, 2009). The general stratigraphy of the field is illustrated in Fig. 1.

The Early Silurian shales of Sarchahan and Siah formations are known as source rocks of the SPGF (Kamali & Rezaee 2003; Aali *et al.*, 2006). The hydrocarbon generation from these source rocks is believed to begin in the Middle Jurassic and the gas window established during early to Middle Cretaceous (Bordenave & Burwood, 1990). The Kangan and Dalan formations are capped by the Triassic age evaporites of Dashtak Formation that forms an efficient cap rock in the region (Fig. 1). These formations host part of the world's largest gas reservoir in the Middle East region. Limestone and dolomite with evaporitic series are the main lithological unit in these formations and are interpreted as shallow-marine deposits (Kashfi, 1992).

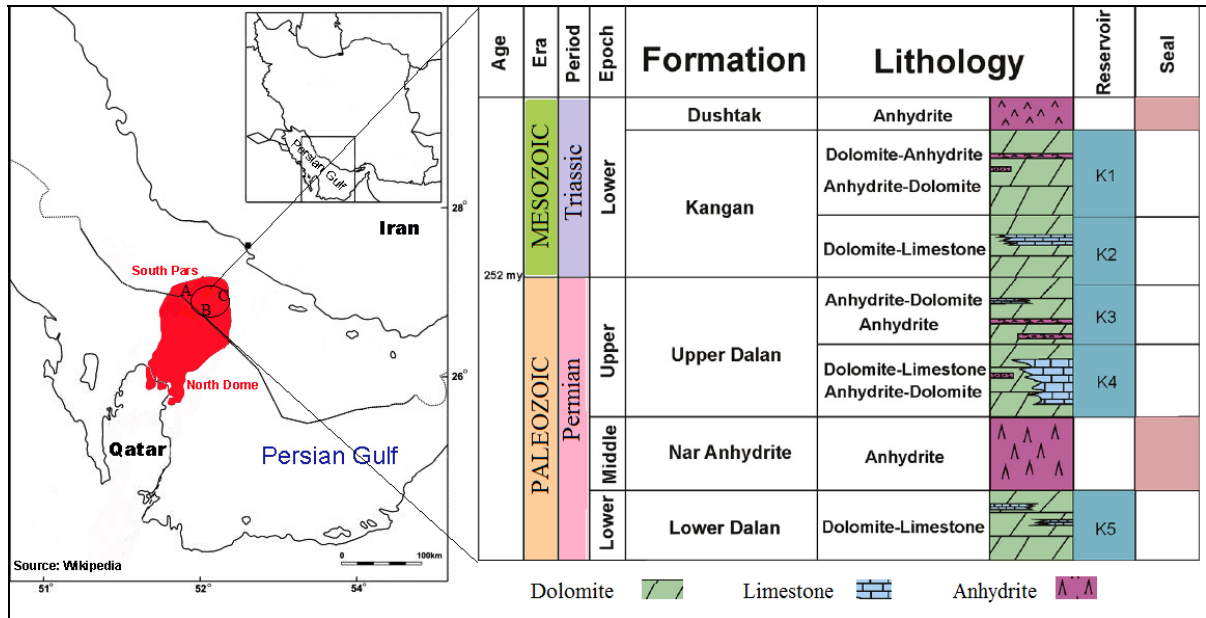


Figure 1. Location map of the South Pars gas field in the Persian Gulf (left) and lithostratigraphic diagram of the studied formations (right)

From a reservoir point of view, the Kangan and Dalan formations are divided into five units. K1 and K2 are two units of Kangan Formation (from top to base), while K3 to K5 are units of Dalan Formation (from top to base). An Anhydrite unit (Nar Member) divides the Dalan Formation stratigraphically to upper (K3 and K4) and lower (K5) Dalan (Figure 1; Ghazban, 2007; Szabo & Kheradpir, 1978).

**Materials and method**

*Data preparation*

Core and petrophysical data from Kangan-Dalan (Late Permian-Early Triassic) formations of the South Pars Field from the Persian Gulf were chosen to test the methodology. Data used in this study come from three wells of the South Pars gas field (SP-A, SP-B and SP-C) and comprise a total of 670 core porosity-permeability sets, 109 MICP curves and 430 thin sections from the K1, K2, K3 and K4 units. The standard thin sections (typically ~30 μm) impregnating with blue epoxy resin to identifying pore space distribution. Identification of dolomite was performed colorimetrically using Alizarin Red-S. Parameterization of the MICP curves with the aim of clustering and pore facies analysis was carried out. The hierarchical cluster analysis method was applied to clustering the PC curves into distinct pore facies. Based on core plug thin-sections, the primary depositional facies and its

diagenetic overprints for each pore facies were determined. In addition, a complete set of well logs including, caliper (CALI), gamma ray (GR), computed gamma ray (CGR), standard gamma ray (SGR), acoustic transmit-time (DT), neutron (NPHI), density (RHOB), photoelectric log (PEF), effective porosity (PHIE) and velocity deviation log (VDL) were available for three wells of the study area. Finally, the GMDH-type (GS-GMDH) neural networks were used to extract pore facies from well log responses. Initially, CALI, GR, CGR, SGR, DT, NPHI, RHOB, PEF, PHIE and VDL logs were considered as inputs and pore facies as the output of the GMDH-NN model to establish a relationship between wireline logs and a set of predefined pore facies which were determined based on clustering of MICP extracted parameters.

*MICP parameter extraction*

Some of the extracted attributes on which the pore facies analysis has been applied are described below.

Pore throat radius can be calculated by using capillary pressure equation (Eq.1) at any capillary pressure.

$$r = \frac{2\sigma (\cos\theta)}{P_c} \tag{1}$$

Where  $r$  is pore throat size in micron,  $\sigma$  is mercury interfacial tension in air in dyn/cm,  $\theta$  is the contact angle between mercury and air in degree and  $P_c$  is

the capillary pressure in kPa.

Height above Free Water Level (HAFWL) directly determines the boundary from which hydrocarbons saturation increases upward. In reservoir conditions, capillary pressure controls the initial hydrocarbon distribution as a function of Height above Free Water Level (HAFWL). Using this principle, the column above zero capillary pressure (free water level) can be determined. The height above free water level is calculated as follows.

$$H = \frac{0.102 P_c}{(\rho_w - \rho_h)} \quad (2)$$

Where,  $H$  is height above free water level (m),  $P_c$  is the capillary pressure in kPa,  $\rho_w$  and  $\rho_h$  are water and hydrocarbon densities under reservoir conditions, respectively. As seen in the formula, there is a direct relation between capillary pressure and hydrocarbon column height.

Swanson's Parameter (SP) is a point in mercury injection presenting the throats which are continuous and plays the main role in fluid flow. Swanson (1981) recognized this point using a cross plot of mercury saturation against the ratio of mercury saturation to injection pressure. The curve maximum point indicates the least pressure values for injecting the mercury and consequently the Swanson's parameter. As mentioned, visionary methods are usually applied to determine this parameter from introduced cross plot.

Pore Throat Sorting (PTS) is mostly applied to calculate and qualify the geometry and sorting of reservoir units throats (Jennings, 1987). Different equations are introduced to calculate PTS. One of these equations applies capillary pressure of first (25% mercury saturation) and third (75% mercury saturation) quartile pressure of MICP curve (Trask, 1932).

$$PTS = \left[ \frac{P_{c75}}{P_{c25}} \right]^{1/2} \quad (3)$$

Where,  $P_{c75}$  is capillary pressure in 75% mercury saturation and  $P_{c25}$  is capillary pressure in 25% mercury saturation.

This formula only covers half of capillary pressures and ignores the trails of the curve. Eq. (4) has a better data coverage, yields more comprehensive results and uses the capillary pressures in 16%, 50% and 84% mercury saturations (Chehrazai et al., 2011):

$$PTS = \frac{P_{c16} + P_{c50} + P_{c84}}{3} \quad (4)$$

As PTS increases, the pore throats sorting and quality decrease and much more injection pressures must be applied to intrude the mercury into porous network.

Pore Throat Size Distribution (PTSD) is a very valuable parameter in the studies about structure and characteristics of pore spaces. This parameter is presented in a graph which is composed of pore throat radius versus normalized pore throat size distribution (PTSD) function. To achieve such a graph, first a plot of mercury saturated pore volume fraction ( $V$ ) versus pore throat size must be constructed, then, the differential of this graph results in PTSD function. Now, the function results a range from 1 to 0 for all pore throat radii. Designed PTSD graph also yields the most frequent radius and the porous network sorting. Eq. (5) is applied to organize the PTSD graph.

$$PTSD = \frac{dv}{d \log(r)} \quad (5)$$

Where  $v$  is the mercury saturated pore volume and  $r$  is pore throat size in micron.

Reservoir Quality Index (RQI) is an important parameter for assessment of reservoir quality based on the routine core analysis (RCAL) data. Reservoir quality index is the estimation of the average hydraulic radius of the reservoir rock. RQI is the particular parameter to determine the flow zone indicator and link the porosity, permeability and capillary pressure together.

Flow Zone Indicator (FZI) is the main parameter to introduce Hydraulic Flow Units HFUs, which is defined based on the reservoir quality index (RQI) and normalized porosity ( $\epsilon$ ) (Amafulle et al., 1993). These parameters must have the most resemblance in categorized units to be able to separate the units according to their flow attitude (Amafulle et al., 1993; Ebanks, 1987; Soto and Garcia, 2001). Flow zone indicator (FZI) and RQI are linked as follows:

$$RQI = 0.0314 \sqrt{\left(\frac{Q}{K}\right)}, \epsilon = \left(\frac{Q}{1-Q}\right), FZI = \frac{RQI}{\epsilon} \quad (6)$$

### Cluster analysis

Cluster analysis is spread to classify a dataset into groups or distinct clusters of data. Clusters are formed in such ways that are internally homogeneous and externally isolated. Many algorithms have been reported in literature among

them Hierarchical Clustering analysis which is used in this study. This method consists of following steps (Sfidari *et al.*, 2012).

1. Calculating the similarity or distance between each two individual data. Particularly, the similarity between two sample vectors is measured based on the distance. Many algorithms have been developed to calculate this parameter among which Euclidean is popular (Eq 7).

$$d_{rs} = \left\{ \sum_{j=1}^n |x_{rj} - x_{sj}|^2 \right\}^{1/2} \quad (7)$$

where,  $x_{rj}$  and  $x_{sj}$  are the  $j$ -th object in clusters  $r$  and  $s$ , respectively.

2. Linking the objects together until one cluster remains

At first, each object is considered as its own cluster. By having similarity or distances between different variables, a combination rule is needed to link objects together and form a union cluster. Various algorithms exist as, single linkage, complete linkage, average linkage, median linkage and Ward linkage

$$d_{(rs)}^2 = \frac{\|\bar{x}_r - \bar{x}_s\|^2}{(n_r + n_s)^s} n_r n_s \quad (8)$$

where,  $n_r$  and  $n_s$  are the number of objects in clusters  $r$  and  $s$ , respectively. Moreover,  $\bar{x}_r$  and  $\bar{x}_s$  are the centroids of clusters  $r$  and  $s$ .

3. Finding where to put the hierarchical tree into clusters.

In this step, a clustering tree is constructed using the information resulting from data connection degree which places them into associated classes. After constructing the dendrogram we can analyze it to select the optimum number of clusters for the dataset by selection of a suitable level of the cutoff. This methodology, i.e. Hierarchical Clustering Analysis (HCA), is developed for the purpose of clustering dominant pore facies hidden in the reservoir.

#### GMDH type neural networks

Group method of data handling (GMDH) is a family of inductive algorithms for mathematical modeling of multi-parametric datasets that present fully automatic structural and parametric optimization of models. By means of the GMDH algorithm, a model can be represented as a set of neurons in which different pairs of them in each layer are connected through a quadratic polynomial

and, thus, produce new neurons in the next layer. Such representation can be used in modeling to map inputs to outputs. The GMDH-type neural networks can organize the optimum multilayered neural network architecture by using the heuristic self-organization method. In each layer, numerous intermediate variables are combined with each other to generate the optimum neuron architectures. The intermediate variables are the outputs of the previous layer. In order to map inputs to outputs in modeling applications, such representation can thus be useful.

Therefore, minimizing the square of the differences between the actual output and the predicted one is the main problem to determine a GMDH type neural network. There are many different possible ways to achieve this goal. The most popular connective function between the inputs and the output variables used in GMDH is the gradually complicated Kolmogorov-Gabor polynomial or Volterra series (Farlow, 1984) which can be expressed in the form of (9)

$$y = a_0 + \sum_{i=1}^n a_i x_i + \sum_{i=1}^n \sum_{j=1}^n a_{ij} x_i x_j + \sum_{i=1}^n \sum_{j=1}^n \sum_{k=1}^n a_{ijk} x_i x_j x_k + \dots \quad (9)$$

A system of quadratic polynomials represents this full form of mathematical explanation by only two variables (neurons) in the form of

$$\hat{y} = G(x_i, x_j) = a_0 + a_1 x_i + a_2 x_j + a_3 x_i x_j + a_4 x_i^2 + a_5 x_j^2 \quad (10)$$

Developing the general mathematical connection between inputs and output variables given in (9) has been a crucial step in the present study and quadratic description was recursively applied in a network of connected neurons to achieve this aim. The differences between real output and predicted one for all input variables are minimized by applying the regression techniques (Farlow, 1984; Iba *et al.*, 1996; Ivakhnenko, 1971) for computing the coefficients  $a_i$  in (10).

The General Structure of GMDH-type neural network (GS-GMDH) has been proposed in literature by many authors (Farlow, 1984; Iba *et al.*, 1996; Ivakhnenko, 1971; Jamali *et al.*, 2009; Nariman-Zadeh *et al.*, 2003) and is used in this work for the purpose of identification and analysis of pore facies. Also, genetic algorithm (GA) is deployed for optimal design of connectivity configuration of such GMDH-type networks and simultaneously, the values of coefficients of quadratic sub-expressions are determined by using

Singular Value Decomposition (SVD).

Training error and prediction error of GMDH-type network are considered as conflicting objective in Pareto optimization process. To construct a multi-objective optimal plan for the generalized structure of the GMDH-type neural network, a multi-objective Uniform-Diversity Genetic Algorithm procedure (MUGA) (Jamali *et al.*, 2008; Jamali *et al.*, 2010; Nariman-Zadeh *et al.*, 2010) is applied and handled in this study. More detailed description of MUGA is reported in (Jamali *et al.*, 2008; Jamali *et al.*, 2010; Nariman-Zadeh *et al.*, 2010).

### Pore facies determination

The Figure 2 exhibits porosity, permeability, and 109 MICP curves from 3 wells in the South Pars Gas Field. A wide range of porosity and permeability with different reservoir quality and MICP curves can be seen in this figure. Since a wide range of the capillary pressure via water saturation is covered in MICP curves, the classification of these curves using graphical examination solely is almost impossible. However, the MICP extracted parameters can be classified into a number of particular pore facies by application of the clustering methods. Cross-plots of various extracted parameter from MICP curves versus permeability are displayed in Figure 3 and Figure 4. Cross-plot of porosity versus permeability for the studied reservoir is displayed in Figure 4. As expected, the correlation coefficient between permeability and extracted MICP parameters is much larger than that of porosity. Among the all MICP extracted parameters,  $R_{35}$  shows a higher correlation with permeability ( $R^2=0.57$ ) (Lucia, 2007), while

Swanson parameter is associated with the lowest correlation as high as 0.24. Moreover, reservoir quality index (RQI) and flow zone indicator (FZI) were evaluated from the result of routine core analysis including porosity and permeability of the 109 core samples. The correlation of the FZI and RQI with permeability is shown in Figure 4 which evidences a good dependence between permeability and RQI/FZI data (Lucia, 2007).

In the current study, pore facies were analyzed through performing clustering analysis of MICP extracted parameters along with porosity, permeability, RQI and FZI data. At first step, the distance between all objects (109 objects) was calculated by applying a suitable distance calculation function (Euclidean distance). Then, various possibilities have been applied for linking the objects based on the result of the distance matrix and comparing the result of these possibilities with another. Finally, the ward method (Ward, 1963) has been selected as a final method for linking the objects. As seen from the extracted dendrogram of Figure 5, the optimum number of clusters can be identified by selecting a suitable cut-off level. Accordingly, five pore facies were defined based on the dendrogram model. The results of the pore facies analysis including the average values of the extracted parameters within each pore facies along with permeability, porosity, RQI and FZI are presented in Table 1 and Figure 6. MICP curves provide pore throat sorting. Well-connected pore system along with good to very good pore throat sorting reflected from mercury injection capillary pressure curves which have lowest displacement pressure and a broad plateau from the low capillary pressure.

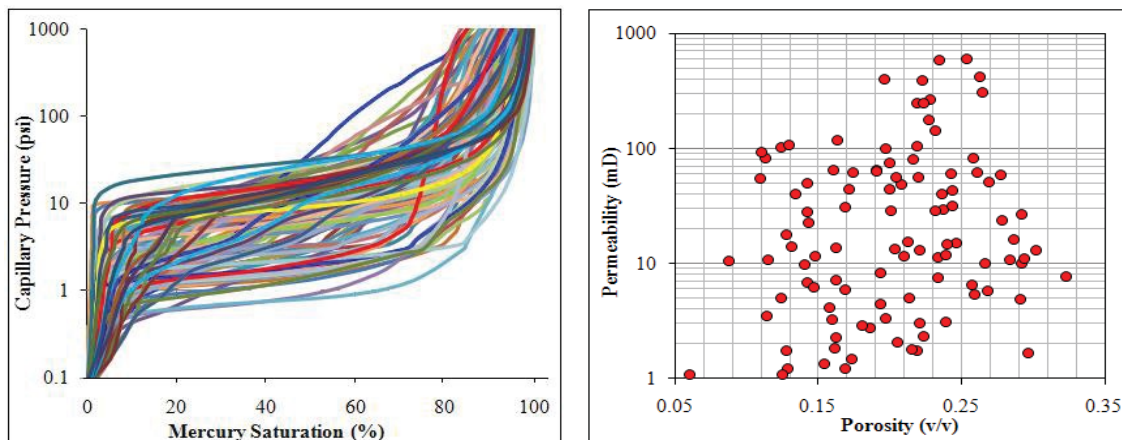


Figure 2. MICP curves from three wells (left), porosity vs. permeability cross-plot of the samples (right).

Table 1. Pore facies clustering results. The average value of the extracted parameters from MICP curves along with porosity and permeability, RQI and FZI in each pore facies are displayed.

	R15	R35	R50	R84	SP	PTS	H_Pc_50	RQI	FZI	Porosity	Permeability
Pore Facies_1	11.28	8.31	6.33	1.00	23.24	6.17	504.92	0.83	3.4	0.204	241.25
Pore Facies_2	4.99	2.68	1.71	0.49	11.98	2.4	1548.63	0.28	1.22	0.205	22.39
Pore Facies_3	3.37	1.32	0.86	0.19	13.20	1.47	6153.53	0.21	1.11	0.193	12.83
Pore Facies_4	3.88	1.23	0.52	0.12	12.71	1.58	23321.29	0.19	0.86	0.190	9.28
Pore Facies_5	0.80	0.24	0.12	0.04	15	0.32	31086.78	0.17	0.67	0.220	6.43

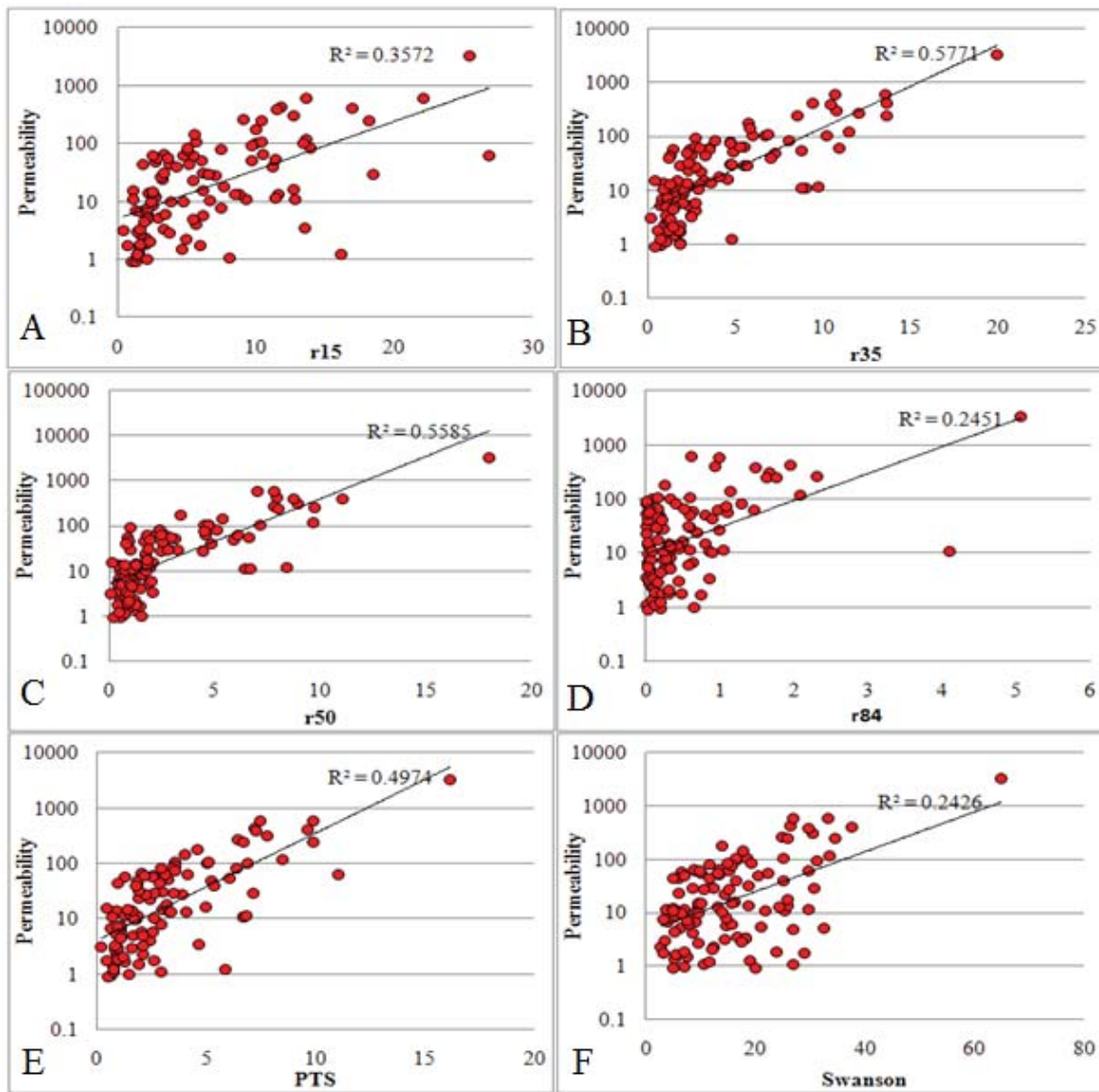


Figure 3. Correlation of the extracted parameters from MICP with permeability. Pore throat radius at equivalent pressure of 15% mercury saturation (A), 35% mercury saturation (B), 50% mercury saturation (C) and 84% mercury saturation (D). Correlation of the permeability with PTS (E) and permeability with Swanson (F)

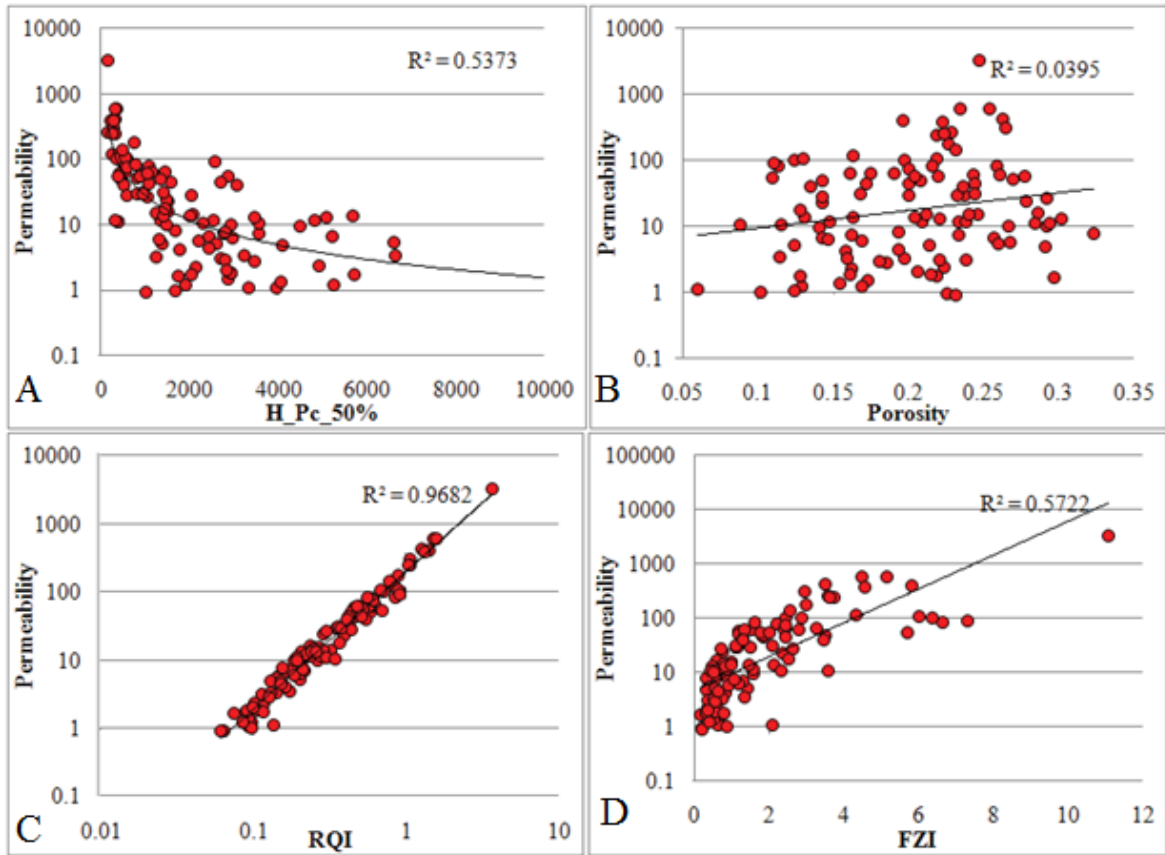


Figure 4. Correlation of the permeability with extracted parameters from MICP and petrophysical data. Correlation of the height above free water level at 50% mercury saturation with permeability (A), correlation of porosity and permeability (B), RQI via permeability (C) and FZI against permeability (D)

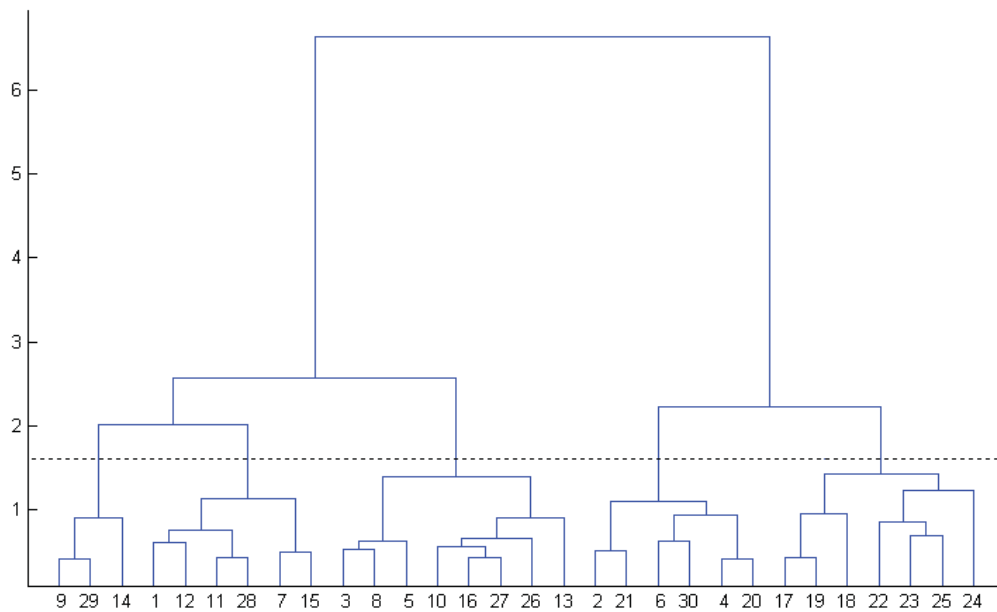


Figure 5. Dendrogram extracted from MICP parameterization data by using HCA method.

Smaller pore throats result in an increase in the slope of the MICP curves. It requires higher pressure for fluid movement among them and finally, it decreases the ability of a pore system to conduct fluids. Depositional facies and subsequent diagenetic over print controlled the pore system and shape of the MICP curves in the studied carbonate rocks. The main characteristics of

each pore facies are interpreted as follows.

Pore facies1: Table 1 shows the petrophysical parameters and pore geometry specifications for each particular pore facies. From this table, we can conclude that pore facies1 has best reservoir quality among the five pore facies. Figure 7a-b points out low displacement pressure in this pore facies which along with flat plateau in low-pressure exhibit good pore system connectivity.

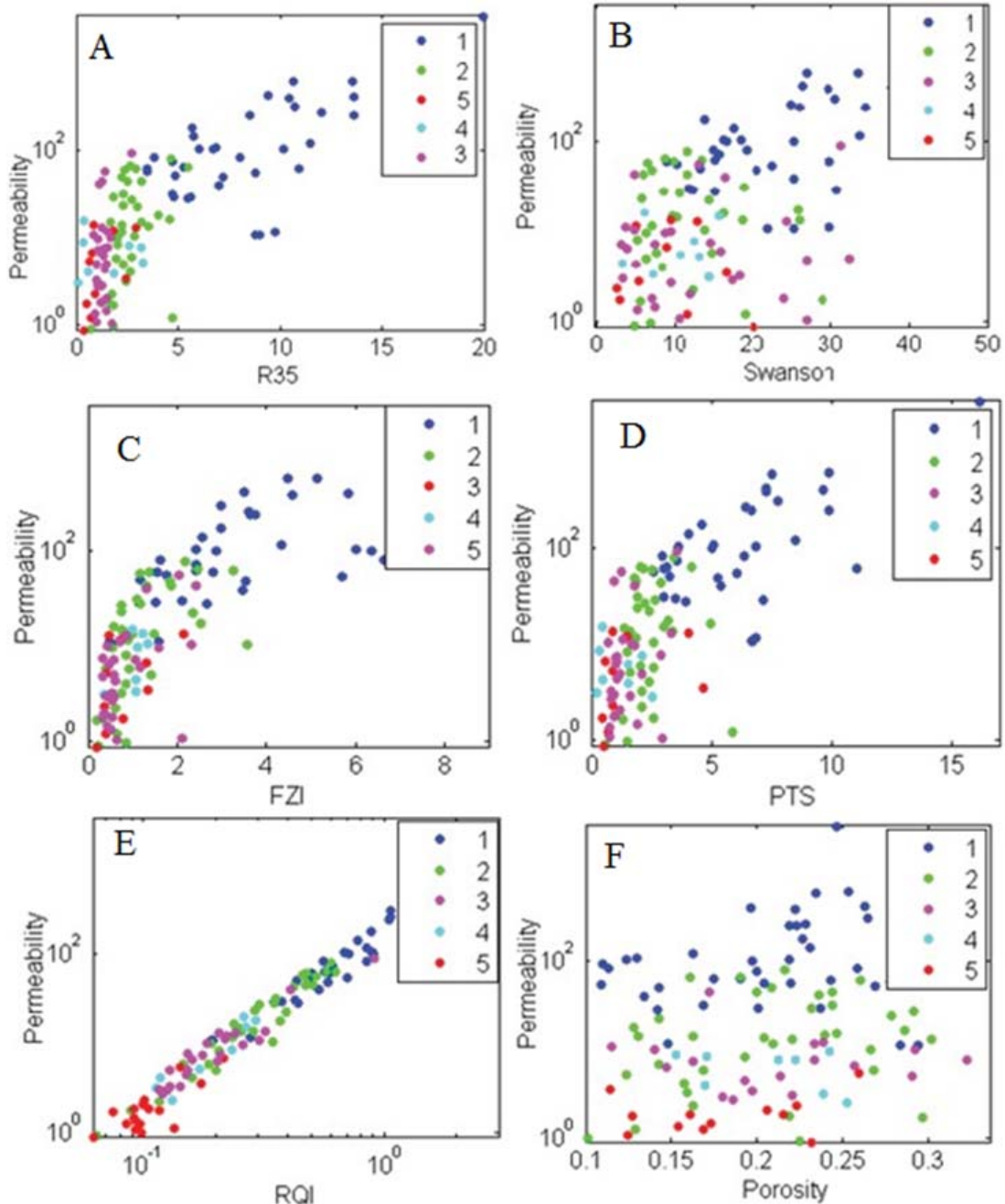


Figure 6. Distribution of input variables used for the clustering with permeability in the each pore facies.

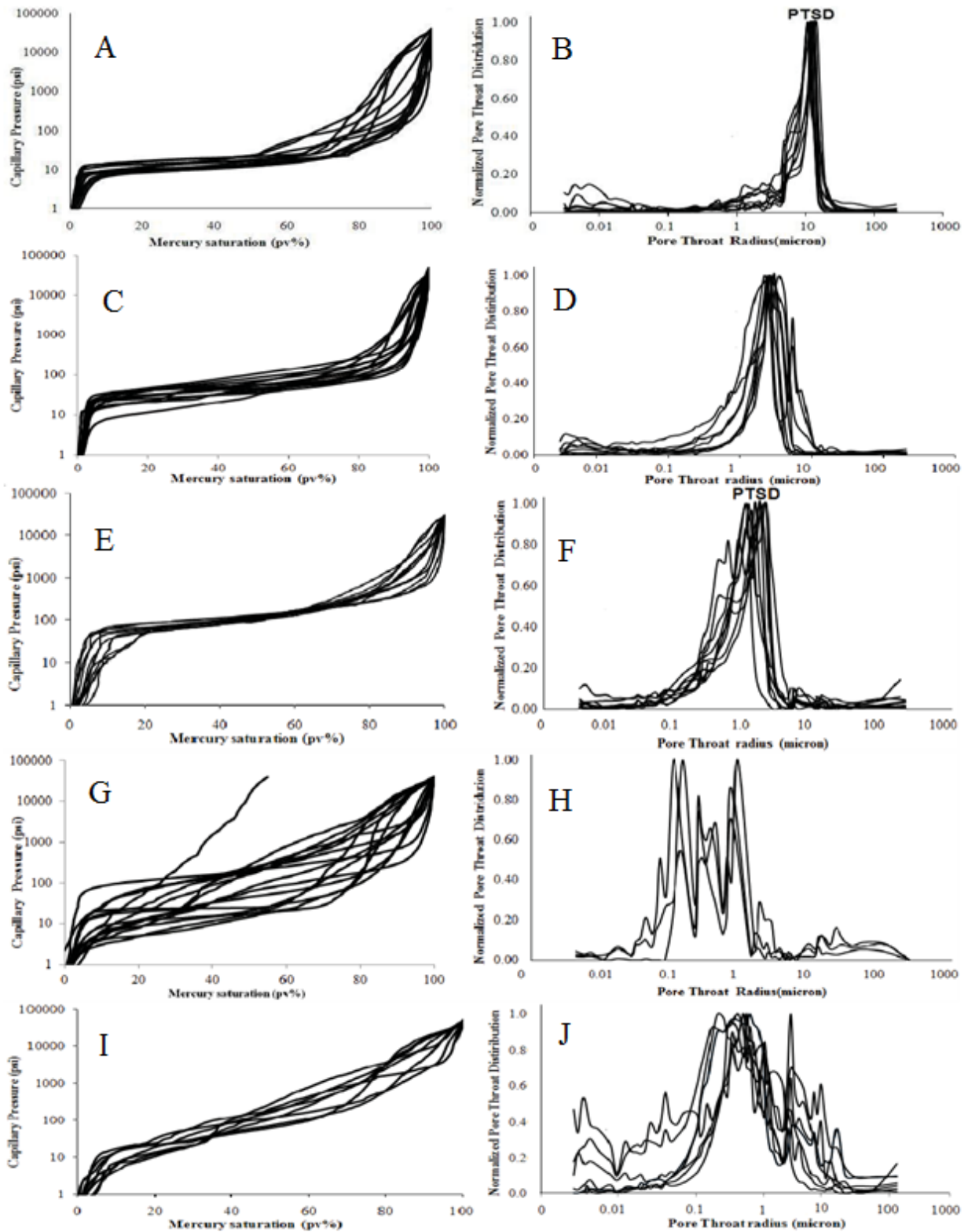


Figure 7. Clustered MICP curves in the five distinct pore facies. Facies 1 (A, B); facies 2 (C, D); facies 3 (E, F); facies 4 (G, H); facies 5 (I, J).

The interesting observation for this facies is that good porosity with large pore throats explains high permeability. These illustrations indicate highest reservoir quality of this facies related to the other ones. The rock fabric and petrographic properties of this facies are shown in Figure 8a and Figure 9a. Porous and permeable compacted coarse-grained

well-sorted peloidal grainstone with well-connected interparticle porosity typical of this pore facies. The main diagenetic overprints are secondary dolomitization and micritization. The main pore type observed in this pore facies is the antiparticle porosity (Figure 8a and Figure 9a).

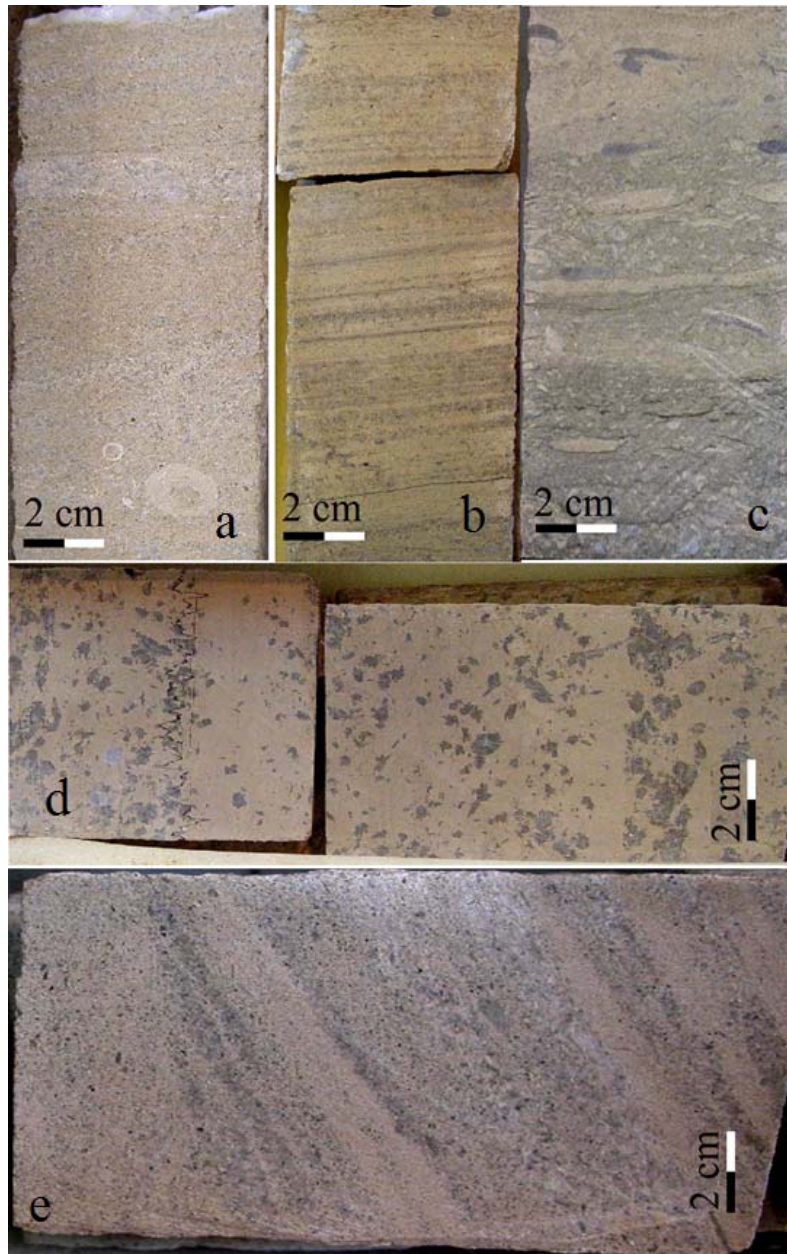


Figure 8. Core slab from the five pore facies in this study. (a) Coarse-grained skeletal ooid grainstone with fining upward forests, skeletal debris is present at the bottom. Ooid shoal setting. (b) Dolomitized cross-bedded peloid/ooid grainstone with dolomitic cement, sparse moldic porosity. Ooid shoal facies. (c) Dolomitic skeletal wackestone to packstone, pore-filling anhydrite is visible. Lagoonal facies. (d) Dolomitic light cream laminated mudstone with pervasive evaporate casts, stylolite is present. Hypersaline lagoonal facies. (e) Oncooid/ooid grainstone with significant moldic porosity at the top and peloidal wackestone to packstone at the bottom, coarsening upward. Lagoonal shoal margin setting.

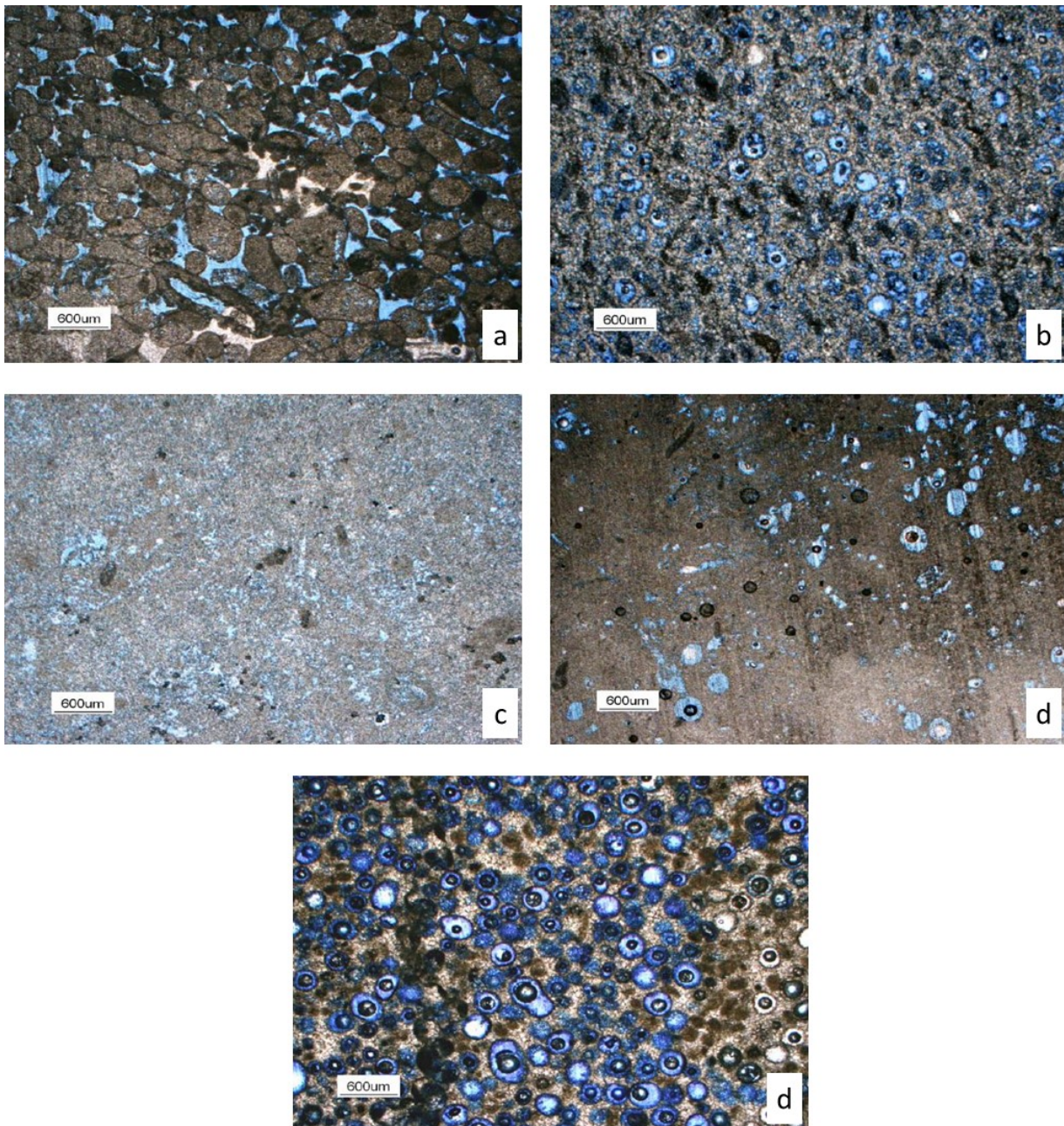


Figure 9. Rock fabric and pore type of the pore facies1, 2, 3, 4 and 5. (a) Coarse-grained well-sorted peloidal grainstone with well-connected interparticle porosity; (b) Well-sorted medium grained moldicoiddolo grainstone. Interparticle pore space was filled with euhedral dolomite cement; (c) Dolomitic peloid wackestone with patchy pore-filling anhydrite. Intercrystalline pore type dominates; (d) Bioturbated skeletal and oolitic wackestone with dolomite moldic, vuggy and microporosity; (e) Ooid-peloidal dolograins with main moldic pore type.

Pore facies2: the average porosity and permeability in pore facies2 are 20% and 22.39 mD, respectively. A platy and flat curve between 10% and 80% saturations demonstrate a uniform pore throat sorting and distribution. PTSD curves are leptokurtic, suggesting an unimodal distribution and a good pore throat sorting (Figure 7c-d). The

dominant pore throat radius ranges from 1 to 8  $\mu\text{m}$ . Well-sorted medium grained moldicoiddolo-grainstone is characteristic of this pore facies. Interparticle pore space was filled with euhedral dolomite cement, with significant intercrystalline porosity. Large moldic pores are connected through the seintercrystalline pores, which display smaller

throat radii than the interparticle pores of pore facies 1. Graphical illustrations are shown in Figure 7, 8b and 9b.

**Pore facies 3:** In comparison with pore facies 1 and 2 it indicates a smaller and less well-sorted pore throat system (Figure 7e-f). The PTSD curves are leptokurtic. The pore throat radius at 80% of the pore volume are located between 0.1 and 6  $\mu\text{m}$  with an average of 1  $\mu\text{m}$ . Dolomitic peloid wackestone with patchy pore-filling anhydrite is the main rock fabric in pore facies 3. As seen in Figure 8c and Figure 9c, intercrystalline pore-type dominates. The average permeability and porosity are 12.83 md and 19% respectively.

**Pore facies 4:** In comparison with the pore facies 1, 2 and 3 there is no flat plateau portion in the MICP curves in this pore facies. PTSD curves show polymodal and platykurtic distribution which indicates a wide range of pore throat radius values and unsorted pore throat system. The pore throat radius is less than 1  $\mu\text{m}$  in 90% of the pore volume. Bioturbated skeletal and oolitic wackestone are representative of this facies. The dominant pore types are moldic and meso-microporosity (Figure 8d and Figure 9d). As indicated by MICP curves, molds are connected through microporosity or mesoporosity. Also, these characteristics along with the average permeability and other petrophysical parameters assigned to this facies indicate a relatively poorer reservoir quality in comparison to pore facies 1, 2 and 3 (Figure 7g-h). The average permeability and porosity are 9.28 md and 19%, respectively.

**Pore facies 5:** No flat plateau, sloping and low displacement pressure on the MICP curves are the main characteristic in this pore facies. A polymodal and very poorly sorted pore system reflected from platykurtic PTSD curves. More than 90% of pore throat radius ranges from 0.1 to 8  $\mu\text{m}$  with an average of 0.7  $\mu\text{m}$  in this facies (Figure 7i-j). Ooid-peloidal dolograins are the typical facies. Interparticle pores are totally plugged by calcite cement preventing from significant compaction. Mold is the main pore type, but moldic pores are mostly isolated by the interparticle cement, with the only minor small-sized connection when former dissolved grains were in contact after mechanical compaction (Figure 8e and Figure 9e). Average permeability and porosity are 9.28 md and 19%, respectively. As a result, the reservoir quality of this pore facies is ranked as fifth in the current classification.

### Pore facies prediction

In this paper, the GMDH-type neural networks were used for the purpose of pore facies identification from well log responses. In order to build a polynomial meta-model by using the GMDH-type neural net, a total number of 109 input-output dataset were used. Ten petrophysical parameters including CALI, GR, CGR, SGR, DT, NPHI, RHOB, PEF, Effective PHI and VDL were considered as inputs and the corresponding pore facies were predicted by GMDH neural nets. Input and output data of designed neural network were categorized into two separate sets (train and test) to visualize the prediction accuracy of the structured GMDH-type neural networks. The training set which consists of selected 76 samples out of 109 input-output data pairs are used for training the neural network models by using MUGA. The testing set which includes remaining 33 unanticipated inputs-output data samples during the training process, is exclusively used for testing to demonstrate the prediction capability of such evolved GMDH-type neural network models.

Training error and prediction error as optimization criteria were considered in a Pareto optimization procedure to obtain some important trade-offs among these conflicting criteria. The optimization procedure is performed by using MUGA. A population size of 70 and generation number of 350 was chosen with crossover probability and mutation probability as 0.90 and 0.03, respectively. Consequently, a total number of 5 non-dominated optimum design points as non-dominated optimum neural network models have been obtained and shown in Figure 10 in the plane of objective functions.

As Figure 10 presents, every optimum design point of the Pareto front is non-dominant and is applicable for configuration of the favourable optimal GMDH-type neural network. Obviously, in the Pareto front, choosing a better value for any criterion would cause a worse value for another criterion. It is now desired to find a trade-off optimum design point compromising both objectives. Design point marked by an arrow in Figure 10 representing a GMDH-type neural network model can be optimally chosen from a trade-off standpoint for optimization criteria.

Hence, the designed structure of the evolved 2-hidden layer GMDH-type neural network is depicted in Figure 11. According to Figure 11, among the ten input parameters, there are only six

ones namely; GR, DT, NPHI, RHOB, Effective PHI and VDL appearing in GMDH model. Thus, it can be concluded that the other four parameters of CALI, CGR, SGR and PEF do not affect the

classification process.

The recursive polynomial representations of such model are given by equations (11):

$$Y_1 = 5.06 - 0.58 DT - 0.67 GR + 0.03 DT^2 + 0.06 GR^2 - 0.01 DT \cdot GR \quad (11a)$$

$$Y_2 = 3.14 + 2.1 PHIfefe - 0.02 VDL - 7.47 PHIfefe^2 + 0.001 VDL^2 - 0.004 PHIfefe \cdot VDL \quad (11b)$$

$$Y_3 = 0.1 + 0.28NPHI + 0.001RHOB - 0.025NPHI^2 - 0.0001RHOB^2 - 0.001 NPHI \cdot RHOB \quad (11c)$$

$$Y_4 = 0.77 + 0.08 Y_1 - 0.06 Y_2 + 0.09 Y_1^2 - 0.04 Y_2^2 + 0.16 Y_1 \cdot Y_2 \quad (11d)$$

$$Y_5 = -7.37 + 1.04 GR + 6.28 Y_3 - 0.02 GR^2 - 0.73 Y_3^2 - 0.51 GR \cdot Y_3 \quad (11e)$$

$$Y_6 = 0.22 + 0.46 Y_4 + 0.36 Y_5 + 0.31 Y_4^2 + 0.62 Y_5^2 - 0.93 Y_4 \cdot Y_5 \quad (11f)$$

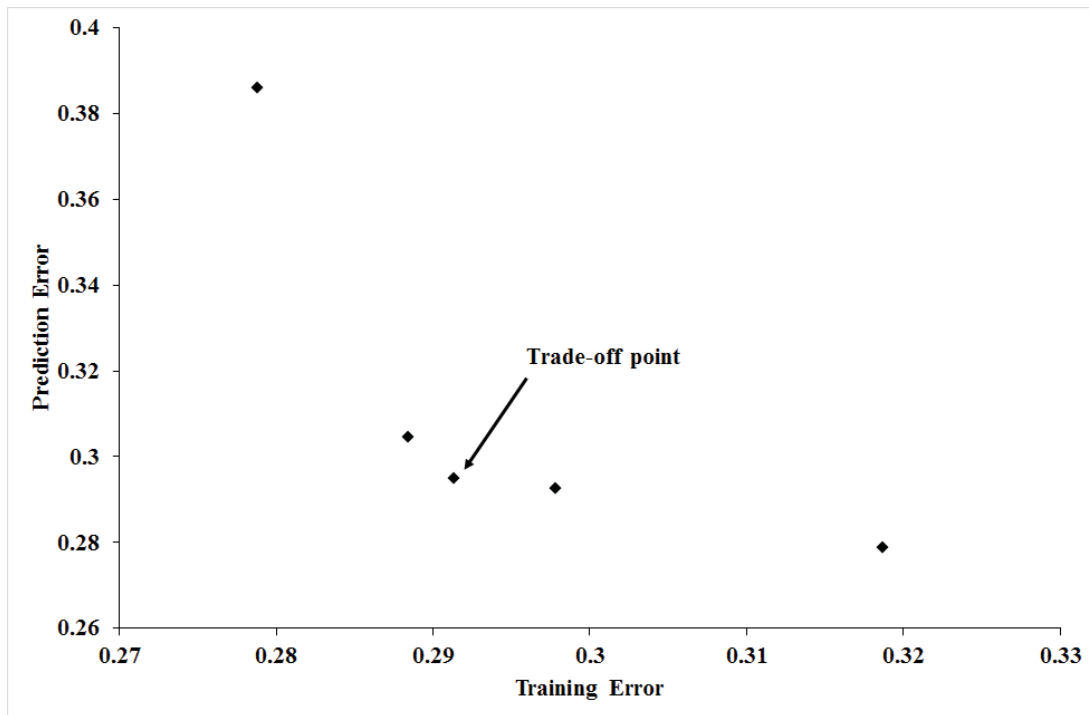


Figure 10. Pareto front of Training error and Prediction error

The accuracy of GMDH model in both training error and prediction error is demonstrated in Figure 12. It is clear from this figure that the proposed meta-modelling GMDH-type neural network of this work notably provides fair estimation and prediction capability in the scope of classification application. Also, it is clearly obvious that the evolved GMDH-type neural network in form of simple polynomial equations can successfully model and predict the output of testing data. The optimized neural network provides nearly 84%

precision in prediction ability for whole data. In the light of the acceptable results of the GMDH type network models, the model with selected parameters from cross-validation and model testing was then used for pore facies prediction in the uncored wells. The outcomes were found in a good performance with reliable prediction effectiveness of the Neural Network classification (Table 2). Figure 13 illustrates a predicted final pore facies in the well scale along with the input well log and porosity-permeability data.

Confusion matrix		predicted litho-facies						Absolute accuracy
		1	2	3	4	5	Grand Total	
Actual facies	1	3	1	0	0	0	4	100
	2	0	5	0	1	0	6	83.33
	3	0	0	4	0	1	5	100
	4	0	0	0	4	0	4	83.33
	5	0	0	0	0	4	4	80
	Grand Total	3	6	4	5	5	23	80
	Proportion percent (%)	75%	100	80%	125%	125%		Absolute accuracy
difference	0	1	0	1	1	3	87.500	

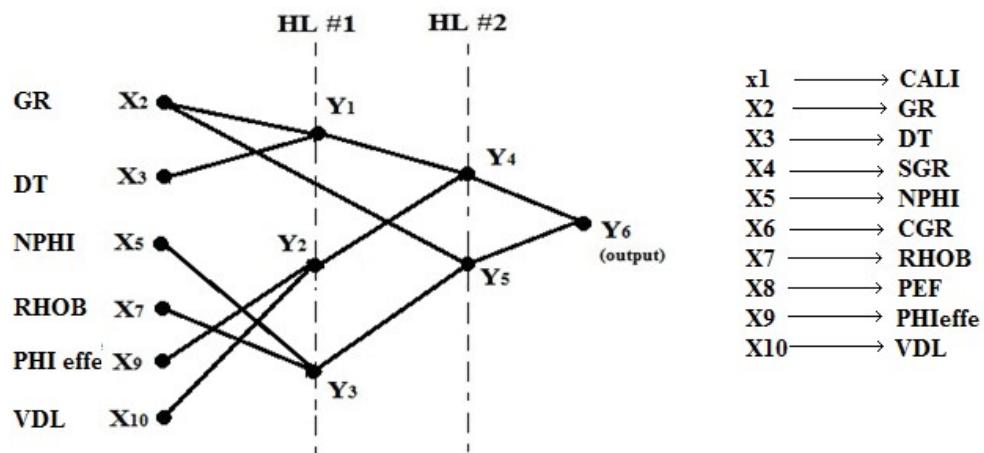


Figure 11. Evolved structure of generalized GMDH neural network

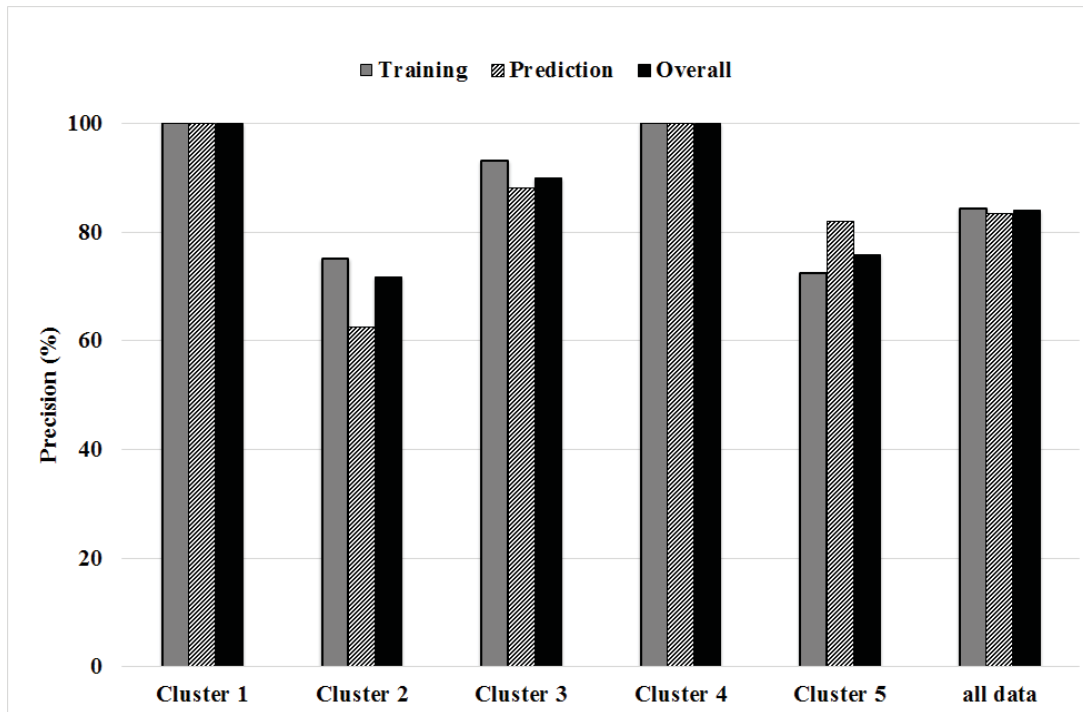


Figure 12. Precision of proposed GMDH-type neural network meta-model

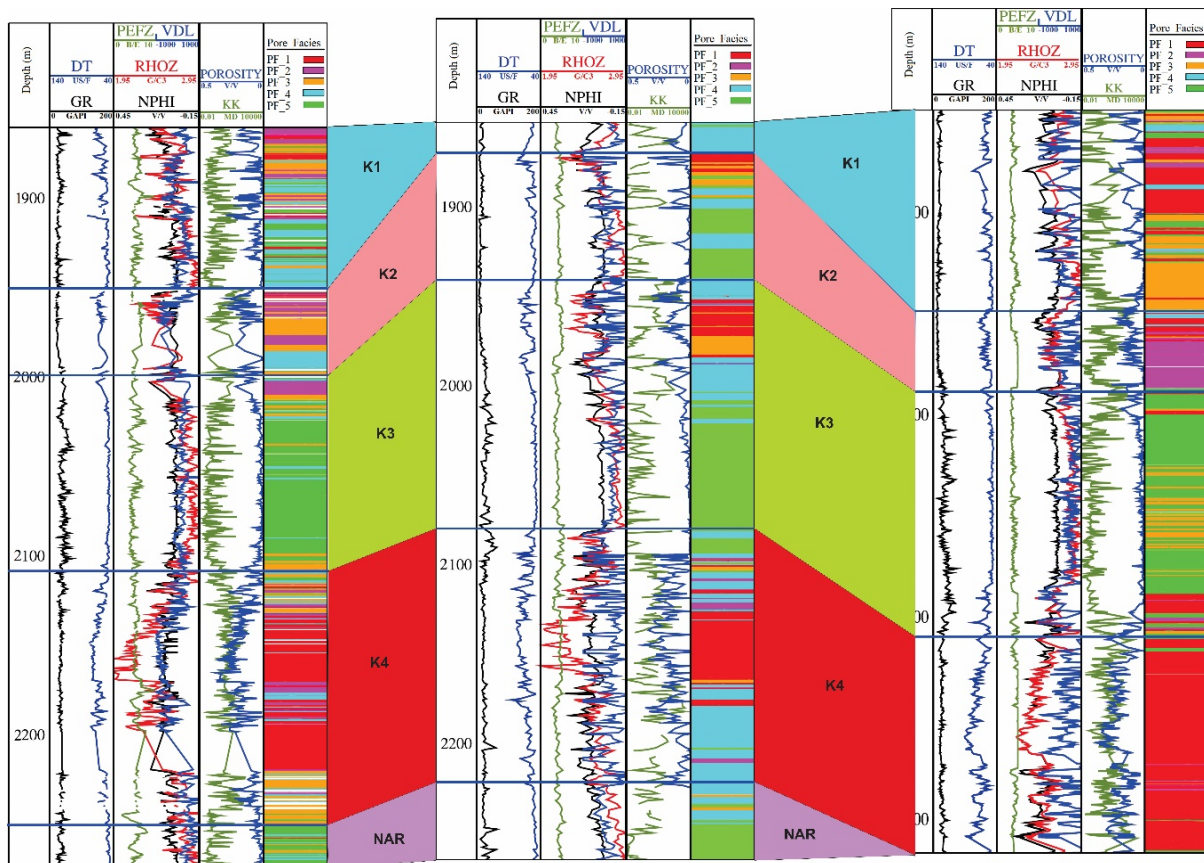


Figure 13. Correlation of the predicted final pore facies in the well scale along with the input well log and porosity-permeability data

## Conclusion

Pore facies analysis plays an important role in the classification of reservoir rocks especially in a carbonate reservoir. In this study, a method is proposed for pore facies determination based on statistical clustering and neural network classification on mercury injection capillary pressure curves, core porosity and permeability data and petrographic and well logs data. Hierarchical clustering analysis method was used for clustering of the pore facies from a set of predefined MICP

data. Five pore facies based on the dendrogram tree were identified, these facies being representative of rocks with different pore geometry, depositional fabrics, diagenetic histories and specific porosity type. Reservoir quality decreases from pore facies 1 to pore facies 5. Evolutionary methods for designing GMDH-type networks were proposed and successfully used for prediction of pore facies from well log parameters. In this way, it has been shown that GMDH-type networks provide effective means for classification of pore facies.

## References

- Aali, J., Rahimpour-Bonab, H. and Kamali, M. R., 2006. Geochemistry and origin of the world's largest gas field from Persian Gulf, Iran. *Journal of Petroleum Science and Engineering*, 50: 161-175.
- Ahr, W.M., 2008. *Geology of Carbonate Reservoirs: the Identification, Description, and Characterization of Hydrocarbon Reservoirs in Carbonate Rocks*. (Hoboken: Wiley), 296 pp.
- Alsharhan, A.S., Nairn, A.E.M., 1997. *Sedimentary Basins and Petroleum Geology of the Middle East*. Elsevier, Netherlands, 843 pp.
- Amaefule, J.O., Altunbay, M., Tiab, D., Kersey, D.G., Keelan, D.K., 1993. Enhanced reservoir description: using core and log data to identify hydraulic (flow) units and predict permeability in uncored intervals/wells. *Society of Petroleum Engineers Paper*, 26436: 1-16.
- Arfi, A. S., Heliot, D., Zhan, J. L. & Allen, D. 2006. A new porosity partitioning-based methodology for permeability and texture analysis in Abu Dhabi carbonates. (SPE paper 101176.) Paper presented at the Abu Dhabi International

- Petroleum Exhibition and Conference, 5–8 November 2006.
- Bordenave, M.L. and Burwood, R., 1990. Source rock distribution and maturation in the Zagros orogenic belt: provenance of the Asmari and Bangestan reservoir oil accumulations. *Organic Geochemistry*, 16(1), 369-387.
- Chehrizi, A., Rezaee, R., Rahimpour-Bonab, H., 2011. Pore facies as a tool for incorporation of small-scale dynamic information in integrated reservoir studies. *Journal of Geophysics and Engineering*, 8: 202–24
- Ehrenberg, S.N., Nadeau, P.H. and Aqrabi, A.A.M., 2007. A comparison of Khuff and Arab reservoir potential throughout the Middle East. *American Association of Petroleum Geologists bulletin*, 91(3): 275-286.
- Ebanks, W.J., 1987. Flow unit concept-integrated approach to reservoir description for engineering projects. *American Association of Petroleum Geologists Meeting Abstracts*, 1: 521-522.
- Farlow, S.J., 1984. Self-organizing methods in modeling: GMDH type algorithms (Vol. 54), Marcel Dekker Inc, CrC Press.
- Ghazban, F., 2007. *Petroleum geology of the Persian Gulf*. Tehran University press, Tehran, 734 pp.
- Iba, H., deGaris, H. and Sato, T., 1996. A numerical Approach to Genetic Programming for System Identification, *Evolutionary Computation*, 3(4): 417-452.
- Insalaco, E., Virgone, A., Courme, B., Gaillot, J., Kamali, M., Moallemi, A., Lotfpour, M. and Monibi, S., 2006. Upper Dalan Member and Kangan Formation between the Zagros Mountains and offshore Fars, Iran: depositional system, biostratigraphy and stratigraphic architecture. *GEOARABIA-MANAMA*, 11(2): 75 pp.
- Ivakhnenko, A.G., 1971. Polynomial theory of complex systems. *IEEE transactions on Systems, Man, and Cybernetics*, 1(4), 364-378.
- Jamali, A., Ghamati, M., Ahmadi, B., & Nariman-Zadeh, N., 2013. Probability of failure for uncertain control systems using neural networks and multi-objective uniform-diversity genetic algorithms (MUGA). *Engineering Applications of Artificial Intelligence*, 26(2): 714-723.
- Jamali, A., Hajiloo, A., and Nariman-zadeh, N., 2010. Reliability-based robust Pareto design of linear state feedback controllers using a multi-objective uniform-diversity genetic algorithm (MUGA), *Expert systems with Applications*, 37 (1): 401-413.
- Jamali, A., Nariman-Zadeh, N., Atashkari, K., 2008. Multi-objective Uniform diversity Genetic Algorithm (MUGA), In *Advanced in Evolutionary Algorithms*, witoldkosinski (Ed.), IN-TECH, Vienna.
- Jamali, A., Nariman-zadeh, N., Darvizeh, A., Masoumi, A., Hamrang, S., 2009. Multi-objective evolutionary optimization of polynomial neural networks for modelling and prediction of explosive cutting process, *Engineering Applications of Artificial Intelligence* 22, (4-5): 676-687.
- Jennings, J.B., 1987. Capillary pressure techniques: application to exploration and development geology. *American Association of Petroleum Geologists*, 71, 1196–1209.
- Kamali, M.R. and Rezaee, M.R., 2003. Burial history reconstruction and thermal modelling at Kuh-e Mond, SW Iran. *Journal of petroleum Geology*, 26(4): 451-464.
- Kashfi, M. S., 1992. Geology of the Permian ‘supergiant’ gas reservoirs in the greater Persian Gulf area *Journal of Petroleum Geology*, 15: 465–80.
- Konyuhov, A.I., Maleki, B., 2006. The Persian Gulf Basin: Geological history, sedimentary formations, and petroleum potential. *Lithology and Mineral Resources*, 41: 344–361.
- Kopaska-Merkel, D.C., Friedman, G.M., 1989. Petrofacies analysis of carbonate rocks: example from lower Paleozoic Hutton Group of Oklahoma and Texas *American Association of Petroleum Geologists Bulletin*, 73: 1289–306
- Lucia, F. J., 2007. *Carbonate reservoir characterization*. Springer, 2nd ed., New York, 226 pp.
- Ma, Z.Y., Wang, H., Sitchler, J., Gurpinar, O., Gomez, E., Wang, Y., 2014. Mixture decompositions and lithofacies clustering from wire line logs. *Journal of Applied Geophysics*, 102: 10–20.
- Marzouk, I., Takezaki, H. & Miwa, M. 1995. Geologic controls on wettability of carbonate reservoirs, Abu Dhabi, U.A.E. Paper presented at the SPE Middle East Oil Show, Bahrain, Manama, 11–14.
- Nariman-Zadeh, N., Darvizeh, A., Jamali, A., Moeini, A., 2005. Evolutionary design of generalized polynomial neural networks for modelling and prediction of explosive forming process, *Journal of Materials Processing Technology*, 164-165 : 1561-1571.
- Nariman-Zadeh, N., Darvizeh, A., Ahmad-Zadeh, R., 2003. Hybrid genetic design of GMDH-type neural networks using singular value decomposition for modelling and prediction of the explosive cutting process, *Proceedings of the Institution of Mechanical Engineers, Part B: Journal of Engineering Manufacture*, 217: 779–790.
- Nariman-Zadeh, N., Salehpour, M., Jamali, A., Haghgoo, E., 2010. Pareto optimization of a five-degree of freedom vehicle vibration model using a multi-objective uniform-diversity genetic algorithm (MUGA), *Engineering Applications of Artificial Intelligence*, 23(4): 543-551.
- Perez, H.H., Datta-Gupta, A., Mishra S., 2003. The Role of Electrofacies, Lithofacies, and Hydraulic Flow Units in Permeability Predictions from Well Logs: A Comparative Analysis Using Classification Trees. *SPE Annual Technical*

- Conference and Exhibition, Denver, Paper 84301-MS, 1–11.
- Rahimpour-Bonab, H., Asadi-Eskandar, A. and Sonei, R., 2009. Effects of the Permian–Triassic boundary on reservoir characteristics of the South Pars gas field, Persian Gulf. *Geological Journal*, 44(3): 341–364.
- Rogers, S. J., Fang, J. H., Karr, C. L., Stanley, D. A., 1992. Determination of lithology from well logs using a neural network. *American Association of Petroleum Geologists Bulletin*, 76: 731–739.
- Saggaf, M.M., Nebrija, Ed. L., 2000. Estimation of lithologies and depositional facies from wire-line logs. *American Association of Petroleum Geologists Bulletin*, 84: 1633–46.
- Serra, O., Delfiner, P., Levertt, J. C., 1985. Lithology determination from well logs: case studies. *Society of Professional Well Log Analysts 26th annual logging symposium. Transactions Paper*.
- Sfidari, E., Kadkhodaie-Ilkhchi, A., Najjari, S., 2012. Comparison of intelligent and statistical clustering approaches to predicting total organic carbon using intelligent systems. *Journal of Petroleum Science and Engineering*, 86–87: 190–205.
- Sfidari, E., Kadkhodaie-Ilkhchi, A., Rahimpour-Bonab, H., Soltani B. 2014. A hybrid approach for litho-facies characterization in the framework of sequence stratigraphy: A case study from the South Pars gas field, the Persian Gulf basin, *Journal of Petroleum Science and Engineering*, 121: 87–102.
- Skalinski, M. T., Gottlib-Zen, S. & Moss, B. 2005. Defining and predicting rock types in carbonates: An integrated approach using core and log data in Tengiz field. Paper presented at the SPWLA 46th Annual Logging Symposium, 26–29.
- Soto, R., Garcia, J.C., 2001. Permeability prediction using hydraulic flow units and hybrid soft computing systems. *SPE* 71455.
- Swanson, B.F. 1981. A simple correlation between permeabilities and mercury capillary pressures, *Journal of Petroleum Technology*, 33: 2488–504.
- Szabo, F., Kheradpir, A., 1978. Permian and Triassic stratigraphy, Zagros basin, south-west Iran. *Journal of Petroleum Geology*, 1: 57–82.
- Tang, H., Ji, H., 2006. Incorporation of spatial characteristics into volcanic facies and favorable reservoir prediction. *SPE Reservoir Evaluation & Engineering*, 9 (5): 565–573.
- Trask, P.D., 1932. *Origin and Environment of Source Sediments of Petroleum* (Houston, TX: Gulf Publishing Company) 323 pp.
- Vincent, B., Fleury, M., Santerre, Y., Brigaud, B. 2011. NMR relaxation of neritic carbonates: An integrated petrophysical and petrographical approach. *Journal of Applied Geophysics*, 74(1): 38–58.
- Ward Jr., J.H., 1963. Hierarchical grouping to optimize an objective function. *Journal of the American Statistical Association*, 48: 236–244.
- Wolff, M., Pelissier-Combes, J., 1982. Faciolog, automatic electro-facies determination. *Society of Professional Well Log Analysts 23rd annual logging symposium. Transactions Paper*.